Photoluminescent ruthenium(ii) bipyridyl complexes containing phosphonium ylide ligands

Oussama Fayafrou, Elise Lognon, Carine Duhayon, Jean-Baptiste Sortais, Antonio Monari, Olivier Baslé, Yves Canac

COMMUNICATION

Photoluminescent ruthenium(II) bipyridyl complexes containing phosphonium ylide ligands

Received 00th January 20xx,
Accepted 00th January 20xx

DOI: 10.1039/x0xx00000x

Oussama Fayafrou,[a] Elise Lognon,[b] Carine Duhayon,[a] Jean-Baptiste Sortais,[a] Antonio Monari,*[b] Olivier Baslé,*[a] Yves Canac*[a]

A P-ylide Ru(II) bipyridyl complex was readily synthetized and fully characterized, constituing one of the rare examples of photoluminescent metal ylide complexes. Its photophysical and redox properties have been compared with those of related NHC and cyclometalated Ru complexes and exploited in visible-light photocatalyzed SET and EnT processes.

Polypyridyl Ru(II) complexes exhibit unique electrochemical and photophysical properties[1] that allow them to be involved in a large variety of applications, such as solar cell implementation,[2] anti cancer treatment therapy[3] or photocatalysis.[4] To improve their overall efficiency, tremendous efforts have been made in ligand design, and in this context, the early introduction of strongly donating carbon ligands was considered. Thus, almost forty years ago, the first cyclometalated phenylpyridine Ru(II) bipyridyl complexes were described,[5] followed by the NHC-based Ru(II) complexes in 2004.[6] Based on this pioneering work, numerous sub-structures incorporating both categories of carbon donors have been characterized, offering the possibility of various substitution pattern, to tune their photochemical properties and extend their field of application.[7] In addition to C-sp^2 anionic aryl- and neutral NHC ligands, another category of carbon ligands, namely phosphonium ylides (P-ylides) has been known for a long time. Beside their essential role in organic synthesis,[8] they were shown to exhibit a rich coordination chemistry with main group elements[9] and transition metals.[10] In fact, P-ylides are neutral 1,2-dipolar molecules with a negatively charged C-sp^3 atom adjacent to a phosphonium. They belong to the familly of η^1-carbon ligands characterized by a strong σ-donor and weak π-acceptor character,[11] and their donor ability is even superior to that of the NHCs.[12] Unexpectedly, while P-ylides have proven useful in homogeneous catalysis,[13] they have so far received very little consideration for the development of photoactive metallic systems. Indeed, with the exception of group XI-based clusters,[14] no examples of molecular P-ylide metal complexes, including in the Ru(II) series, has been the subject of a detailed study concerning its photophysical properties. Moreover, P-ylides have not yet been taken into account in photocatalysis, a field which has experienced enormous success in recent years,[15] leading to the proposition of a plethora of different ligands. In the framework of this emerging domain, our contribution addresses the straightforward synthesis of the first photoluminescent Ru(II) bipyridyl complex [**C**]X_2 containing a chelating phosphonium ylide-pyridyl ligand. This provides also a direct comparison with the parent [Ru(bpy)$_3$]X_2 prototype, and the related cyclometalated [**A**]X[16] and NHC [**B**]X_2[17] Ru(II) bipyridyl complexes (Fig. 1). In addition, electrochemical and photophysical studies, complemented with molecular modeling and preliminary applications in photocatalysis are reported, affording a general overview of the potential of this new type of Ru P-ylide architecture.

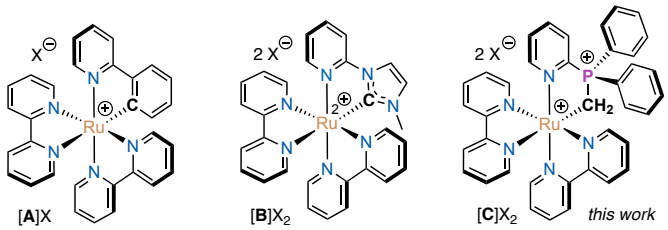

Figure 1. Targeted P-ylide Ru(II) bipyridyl complex [**C**]X_2 with related known cyclometalated phenyl-pyridine [**A**]X and NHC-based [**B**]X_2 Ru(II) bipyridyl complexes.

Access to the targeted P-ylide Ru(II) bipyridyl complex was envisioned from readily available 2-(diphenylphosphino)pyridine **1**. In a first step, we were pleased to observe that the methylation of **1** with MeI in toluene at 90°C occurred selectively at the soft P-center, affording after anion metathesis the phosphonium salt [**2**](PF_6) in 88% yield (Scheme 1). Its structure as well as that of phosphonium intermediate [**2**](I) were confirmed by single-crystal X-ray diffraction (ESI). Then, [**2**](PF_6) was reacted in THF at −78 °C with an equivalent of KHMDS followed by the addition of a stoechiometric amount of [Ru(*p*-cymene)Cl_2]$_2$ dimer. After work-up, the P-ylide Ru(II)(*p*-cymene) complex [**3**](PF_6) was isolated in 67% yield as an orange crystalline air-stable solid. In the ^{31}P NMR spectrum, the presence of a single resonance at chemical shift (δ_P) of 48.9 ppm, deshielded compared to that of precursor [**2**](PF_6) (δ_P 17.0 ppm), confirmed the formation of a Ru coordinated P-ylide. The linkage of the CH_2 ylide was also apparent from the upfield shift of the corresponding ^{13}C NMR resonance with appropriate multiplicity (δ_{CH2} 0.3 ppm, d, $^1J_{CP}$ = 31.3 Hz). The complex [**3**](PF_6) was characterized by X-ray diffraction

[a] *LCC-CNRS, Université de Toulouse, CNRS, UPS, Toulouse, France.*
E-mail: olivier.basle@lcc-toulouse.fr; yves.canac@lcc-toulouse.fr
[b] *ITODYS, Université Paris Cité and CNRS 75006, Paris, France.*
E-mail: antonio.monari@u-paris.fr

† Electronic supplementary information (ESI) available. Synthesis, spectroscopic, crystallographic and catalytic details. CCDC 2382356-2382360
For ESI and crystallographic data in CIF and other electronic format see DOI: 10.1039/x0xx00000x.

showing the presence of a five-membered metallacycle with typical piano-stool geometry (Fig. 2). The Ru–ylide bond (2.1383(18) Å) falls within the range of the rare examples of P-ylide Ru complexes.[18] In a last step, the subsequent displacement of *p*-cymene and chloride co-ligands was achieved by heating [**3**](PF_6) in DMSO at 130 °C in the presence of two equivalents of 2,2'-bipyridine and $AgPF_6$ (Scheme 1). After purification by chromatography on silica gel, the title complex [**C**]$(PF_6)_2$ was isolated in 90% yield as an air-stable dark red solid. Upon exchange at the Ru(II) center (*p*-cymene *vs* bpy), the ^{31}P NMR chemical shift remained essentially unchanged with a singlet at δ_P 45.4 ppm. The persistence of the Ru–CH_2 bond was confirmed by ^{13}C NMR with a doublet signal in the high-field region (δ_{CH2} −0.2 ppm, d, $^1J_{CP}$ = 20.6 Hz). In the ^1H NMR spectrum, the two diastereotopic H-atoms of the [−CH_2–PPh_2Pyr−]$^+$ moiety appeared as a doublet of doublets in the high-field zone (0.9−1.8 ppm). The structure of [**C**]$(PF_6)_2$ was established by X-ray diffraction showing a distorted octahedral geometry around the Ru center with the *N,C*-chelating pyridyl-ylide ligand which forms a five-membered metallacycle (Fig. 2). The Ru–ylide bond (2.145(5) Å) is significantly longer than Ru–NHC (1.97-2.00 Å)[17a] and Ru–phenyl (2.044(1) Å)[19] bonds in corresponding complexes, consistent with their respective hybridization state (C-sp^3 vs C-sp^2). The CH_2 ylide points out of the plane defined by the other four atoms pushing back one of the pyridine which induces the lengthening of the Ru–N2 bond (2.088(4) Å). Compared to Ru–N4 and Ru–N5 bond lengths (2.048-2.057 Å), the Ru–N3 bond (2.087(4) Å) also experiences an elongation of 0.03-0.04 Å due to the *trans* influence of the strongly donating ylide. Gratifyingly, adding $AgPF_6$ to [**3**](PF_6) in MeCN at 100°C in the absence of 2,2'-bipyridine led to the formation of the tetra(acetonitrile)pyridyl-ylide Ru(II) complex [**4**]$(PF_6)_2$ isolated in 95% yield as orange air-stable crystals (Scheme 1). As confirmed by X-ray diffraction, [**4**]$(PF_6)_2$ exhibits a typical octahedral geometry with the Ru–N3 bond distance (2.100(5) Å) *trans* to the ylide being elongated compared to the three other Ru–N bonds (2.010-2.025 Å) (Fig. 2). It is worth mentioning that the obtention of [**4**]$(PF_6)_2$ opens perspectives for accessing functionalized P-ylide Ru complexes.

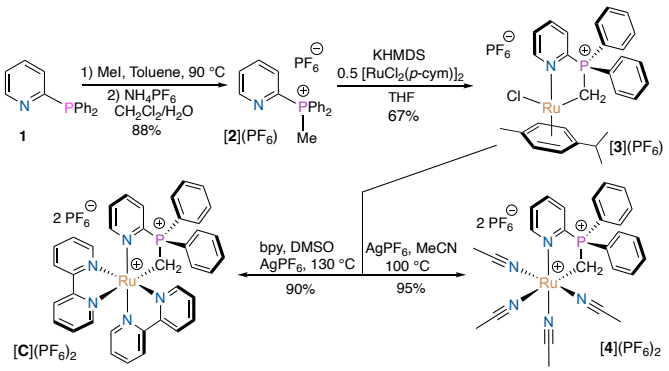

Scheme 1. Synthesis of P-ylide Ru(II) bipyridyl [**C**]$(PF_6)_2$ and tetra-acetonitrile [**4**]$(PF_6)_2$ complexes from 2-(diphenylphosphino)pyridine **1**.

Photophysical and electrochemical properties of P-ylide complex [**C**]$(PF_6)_2$ were evaluated and compared with those of [Ru(bpy)$_3$]$(PF_6)_2$[20] and the structurally related Ru bipyridyl

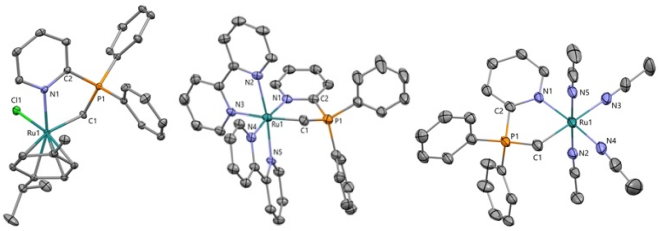

Figure 2. Perspective views of the cationic part of [**3**](PF_6) (*left*), [**C**]$(PF_6)_2$ (*middle*) and [**4**]$(PF_6)_2$ (*right*) with thermal ellipsoids drawn at the 30% probability level. Selected bond lengths [Å], and angles (°). [**3**](PF_6): C1–P1 = 1.7548(19); C1–Ru1 = 2.1383(18); N1–Ru1 = 2.1120(16); Cl1–Ru1 = 2.4004(5); P1–C1–Ru1 = 106.29(9); C1–Ru1–N1 = 84.58(7); [**C**]$(PF_6)_2$: C1–P1 = 1.756(6); C1–Ru1 = 2.145(5); N1–Ru1 = 2.101(4); N2–Ru1 = 2.088(4); N3–Ru1 = 2.087(4); N4–Ru1 = 2.057(4); N5–Ru1 = 2.048(4); P1–C1–Ru1 = 106.4(3); C1–Ru1–N1 = 87.30(19); C1–Ru1–N3 = 175.73(18); C1–Ru1–N4 = 87.06(18); N1–Ru1–N4 = 174.03(16); N2–Ru1–N5 = 171.12(16); [**4**]$(PF_6)_2$: C1–P1 = 1.748(6); C1–Ru1 = 2.124(5); N1–Ru1 = 2.077(5); N2–Ru1 = 2.010(5); N3–Ru1 = 2.100(5); N4–Ru1 = 2.022(6); N5–Ru1 = 2.025(5); P1–C1–Ru1 = 107.0(3); C1–Ru1–N1 = 87.0(2); C1–Ru1–N3 = 177.8(2); C1–Ru1–N4 = 87.8(2); N1–Ru1–N4 = 174.72(19); N2–Ru1–N5 = 177.9(2).

complexes [**A**](PF_6)[16] and [**B**]$(PF_6)_2$[17] of bidentate phenyl-pyridyl and NHC-pyridyl ligands, respectively. The absorption spectrum of P-ylide complex [**C**]$(PF_6)_2$ recorded at room temperature (RT) in DCM at a concentration of 1.10^{-5} mol/L evidenced a strong absorption in the high UV range (295 nm, ε = 56820 M.cm^{-1}) and a broad band of weaker intensity in the visible region with a λ_{max} at 495 nm (ε = 13510 M.cm^{-1}) (Fig. 3, Table 1). By reference to Ru(II) polypyridyl complexes,[1] these absorption bands were assigned to ligand-centered π–π* (LC) and metal-to-ligand charge-transfer (MLCT) transitions (i.e., d -> π* transitions), respectively. Compared to [Ru(bpy)$_3$]$(PF_6)_2$ and the NHC complex [**B**]$(PF_6)_2$, the lowest energy band absorption of [**C**]$(PF_6)_2$ displays a bathochromic shift of about 50 nm. This effect can be rationalized by the stronger donation of the P-ylide which destabilizes the highest-occupied 4d orbitals on Ru decreasing the gap between those orbitals and the bpy π* orbitals in agreement with the MLCT character of this band. The corresponding MLCT absorption band of [**A**](PF_6) was observed at lower energy (λ_{max} = 548 nm) due to the even more donating character of the phenylated ligand. RT emission measurements carried out in DCM, under 495 nm excitation, shown that the ylide complex [**C**]$(PF_6)_2$ is emissive with a single and broad emission band at λ_{max} = 672 nm. In the solid state, [**C**]$(PF_6)_2$ emits at similar wavelengths, although with a slight temperature-dependent blue-shift from 293 to 77 K (λ_{max} = 675 to 670 nm) (SI). In fact, emission wavelengths of [Ru(bpy)$_3$]$(PF_6)_2$ (λ_{max} = 596 nm), [**C**]$(PF_6)_2$ (λ_{max} = 672 nm), [**B**]$(PF_6)_2$ (λ_{max} = 620 nm) and [**A**](PF_6) (λ_{max} = 821 nm) correlate well with the energetic trend observed for the absorption spectra, and therefore with the inherent electronic properties of the corresponding carbon ligands. The excited state lifetime (τ_o = 62 ns) and luminescence quantum yield (Φ_{lum} < 0.01) of [**C**]$(PF_6)_2$ follow the same trend being lower than those of [Ru(bpy)$_3$]$(PF_6)_2$ and NHC complex [**B**]$(PF_6)_2$, but superior to that of cyclometalated complex [**A**](PF_6). The photostability of [**C**]$(PF_6)_2$ was also investigated by measuring the luminescence intensity of a DCM solution irradiated at λ_{max} = 460 nm (Fig. 3). Thus, the photostability of [**C**]$(PF_6)_2$ is slightly lower than that of the [Ru(bpy)$_3$]$(PF_6)_2$ reference, namely a conservation of 80% of its initial luminescence after 1 h of irradiation. The influence of the P-ylide ligand was further investigated by cyclic voltammetry in DCM solution. Complex [**C**]$(PF_6)_2$ exhibits a reversible oxidation wave at $E_{1/2}$ = 0.95 V/ECS for the Ru^{II}/Ru^{III} event and a

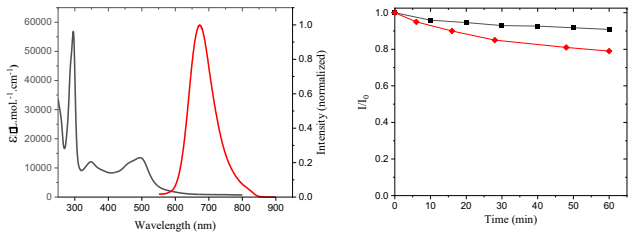

Figure 3. UV-Vis absorption (black line) and emission (red line, λ_{ex} = 495 nm) in CH_2Cl_2 of [**C**]$(PF_6)_2$ (left). Photostability of [Ru(bpy)$_3$]$(PF_6)_2$ (black line) and [**C**]$(PF_6)_2$ (red line) in CH_2Cl_2 at 25 °C under 50W blue LED (λ_{max} = 460 nm) irradiation (right).

reversible reduction at $E_{1/2}$ = –1.46 V/ECS assigned to ligand centered reduction (ESI). Thus, similarly to photophysical data, comparison of these redox values with those of [Ru(bpy)$_3$]$(PF_6)_2$ and complexes [**A**](PF_6) and [**B**]$(PF_6)_2$ clearly reflect the electronic properties of the supported carbon ligands, the neutral C-sp^3 ylide being located in term of donating strength between the neutral C-sp^2 NHC and the anionic C-sp^2 aryl ligand. Notably, the modification of the carbon ligand has more impact on the oxidation than on the reduction events with a direct influence on the HOMO-LUMO gap of complexes, consistent with the luminescence data given in Table 1.

Table 1. Photophysical and electrochemical properties of complex [**C**]$(PF_6)_2$ and comparison with [Ru(bpy)$_3$]$(PF_6)_2$ and carbon-based Ru complexes [**A**](PF_6) and [**B**]$(PF_6)_2$.

Complex	λ_{abs} (nm)	λ_{em} (nm)	τ_0 (ns)	Φ_{lum}	$E^{red}_{1/2}$[g]	$E^{ox}_{1/2}$[g]
[**C**]$(PF_6)_2$[a]	495	672[b]	62[c]	<0.01	–1.46	0.95
[Ru(bpy)$_3$]$(PF_6)_2$[d]	451	596	675	0.05	–1.29	1.40
[**B**]$(PF_6)_2$[e]	445	620	187	0.01	–1.36	1.23
[**A**](PF_6)[f]	548	821	13	<0.005	–1.55	0.47

[a] In dry, degassed CH_2Cl_2 at 293K.[b] λ_{exc} = 495 nm.[c] λ_{exc} = 455 nm.[d] From reference [20]. [e] From reference [17]. [f] From reference [16].[g] Redox potentials (V) against ECS.

To better rationalize these results, we performed molecular modeling and simulation at the density functional theory level. All the three Ru complexes adopt, as expected, a distorted octahedral geometry (ESI). The simulated absorption spectra are collected in ESI with the lowest in energy and most intense individual transitions. Despite a global blue-shift, the experimental trends are correctly reproduced. In particular, the lowest energy band of [**C**] peaks in between those of [**B**] which is blue shifted and [**A**] red shifted with a difference between the absorption maxima of 26 and 41 nm, respectively. Interestingly, and as confirmed by the natural transition orbitals (NTO, Fig. 4), the nature of the low energy states is consistently of MLCT type. In the case of [**C**], the electronic density is accumulated on the bipyridine ligands for the lowest energy band and on the pyridine-ylide backbone at higher excitation energies. The gap between the MC and MLCT states, dictating photostability and excited state lifetime, has been estimated at Franck-Condon (ESI). Even though [**C**] experiences a decrease of the MC/MLCT gap compared to the other complexes, the two states are still sufficiently separate to avoid inversion and hence a dramatic shortening of the lifetime of the MLCT state. As concerns the emission properties (ESI), we may observe a general red-shift of the simulated wavelengths, even if the experimental trends among the different compounds are respected. The modeling of the redox properties of [**C**] evidences that the electron density of the reduced species is accumulated on the ligands (Fig. 4B), and more specifically on the bipyridine units. On the other hand, in the oxidized complex the hole is localized on the d orbitals of the Ru center (Figure 4C). From a quantitative point of view, the energy difference between the two species has been estimated at 2.68 eV in agreement with experimental redox values.

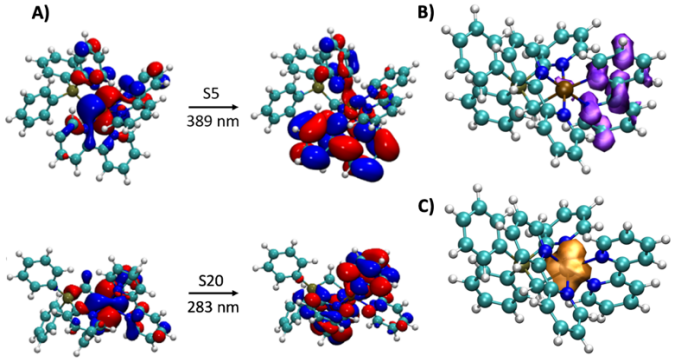

Figure 4. (**A**) TD-DFT NTOS for the most important transitions of complex [**C**], spin density representing the unpaired electron localization for the reduced (**B**) and oxidized (**C**) system of complex [**C**].

Visible light-photocatalysis has recently emerged as a powerful tool for organic synthesis, taking advantage of photoinduced single electron transfer (SET) or energy transfer (EnT) mechanisms, which are respectively governed by the redox potentials and the triplet energy values of excited state species.[21] Since Ru(II) polypyridyl complexes are active photocatalysts in both processes through the involvement of their ^{3}MLCT excited state,[22] we decided to gain some information on the photocatalytic activity of P-ylide Ru complex [**C**]$(PF_6)_2$. Based on a SET mechanism, the oxidative coupling of nitroalkanes with *N*-aryl tetrahydroisoquinolines (THIQ) under visible light irradiation was reported to be a valuable method of functionalizing Csp^3–H bonds adjacent to N-atom.[23] This so-called Aza-Henry reaction was demonstrated to be photocatalyzed by [Ru(bpy)$_3$]Cl_2. Thus, a solution of THIQ and 1.0 mol% of [**C**]$(PF_6)_2$ in $MeNO_2$ was irradiated with blue LEDs (λ_{max} = 460 nm) under O_2 atmosphere. While after 2h, only 37% of product was formed, the Henry adduct was produced in 80% yield after 6 h (Table 2, entries 1-2). Extending the irradiation time to 16 h did not improve the yield (entry 3). As expected, the exclusion of O_2 that acts as external oxidant resulted in a lower yield (entry 4).[24] Performing the reaction in the absence of Ru catalyst led to the product in 30% yield in agreement with the formation of an electron donor-acceptor complex between THIQ and $MeNO_2$ (entry 5).[25] For comparison, under the same conditions, [Ru(bpy)$_3$]$(PF_6)_2$ afforded $MeNO_2$ adduct in only 54% yield (entry 6). In agreement with the redox potential of involved species, the formation of the Henry product can be rationalized by the oxidative quenching of photoactivated ylide catalyst [**C**]$(PF_6)_2$ by O_2 through a Ru(II)/Ru(III) cycle. In a second time, as a photo-induced EnT transformation, we focused on alkene isomerization where the thermodynamically less stable isomer can be generally produced.[26]

Table 2. Aza-Henry reaction and isomerization of *E*-stilbene with [**C**](PF$_6$)$_2$.

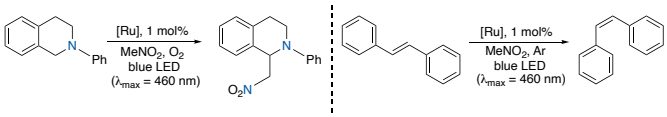

Entry[a]	Catalyst	Time[e]	Yield[d]	Entry[c]	Catalyst	Time[e]	Yield[d]
1	[**C**](PF$_6$)$_2$	2	37	7	[**C**](PF$_6$)$_2$	8	39
2	[**C**](PF$_6$)$_2$	6	80	8	[**C**](PF$_6$)$_2$	16	84
3	[**C**](PF$_6$)$_2$	16	77	9	-	16	0
4[b]	[**C**](PF$_6$)$_2$	16	40	10	[Ru(bpy)$_3$](PF$_6$)$_2$	16	80
5	-	16	30				
6	[Ru(bpy)$_3$](PF$_6$)$_2$	16	54				

[a]Reaction conditions: 0.2 mmol, $MeNO_2$ (1 mL). [b]Under Ar. [c]Reaction conditions: 0.2 mmol, degassed $MeNO_2$ (1 mL). [d]Yield in % was determined by ^{1}H NMR using 1,3,5-trimethylbenzene as an internal standard. [e]Time was given in hours.

Gratifyingly, reacting the *E*-stilbene in $MeNO_2$ in the presence of 1 mol% of [**C**](PF$_6$)$_2$ under blue LED irradiation (λ_{max} = 460 nm) afforded, after 16 h, its *Z*-isomer with an excellent conversion of 84% (entry 8). Noteworthy, a slightly lower conversion (ca 80%) was observed with [Ru(bpy)$_3$](PF$_6$)$_2$ while no reaction occurred in the absence of [**C**](PF$_6$)$_2$ (entries 9-10). The ^{3}MLCT energy of [**C**](PF$_6$)$_2$ estimated from emission spectrum (E_T ~ 43.0 Kcal mol^{-1}) suggests that the isomerization of *E*-stilbene is here slightly endergonic.[27] However, vibronic coupling may favor energy transfer, or state mixing, which will in turn trigger the, downhill, isomerization cascade (ESI).

An air-stable Ru(II) bipyridyl complex of a chelating P-ylide-pyridyl ligand was easily prepared in a three-step sequence from 2-(diphenylphosphino)pyridine. This complex represents one of the very few examples of photoluminescent P-ylide complexes, and the first representative in the Ru series. It displays notably a photoluminescence red-shifted relative to that of [Ru(bpy)$_3$](PF$_6$)$_2$ and in between those of closely related NHC and cyclometalated Ru bipyridyl complexes in accordance with the electronic properties of corresponding carbon ligands. Finally, this P-ylide Ru complex was demonstrated to be active in visible-light photocatalyzed SET and EnT processes, namely the Aza-Henry reaction and the isomerization of *E*-stilbene, which stand as the first photocatalyzed reactions involving P-ylides, thus opening new avenues in this field.

Data availability

The data supporting this article were included as part of the ESI.†

Conflicts of interest

There are no conflicts to declare.

Acknowledgements

This work was supported by the CNRS and the Agence Nationale de la Recherche (ANR-21-CE07-0026 “LYMACATO”). The authors thank G. Molnar from LCC-Toulouse for excited state lifetime measurements and INSA-Toulouse for luminescence quantum yield measurements.

Notes and references

1 Q. Sun, S. Mosquera-Vazquez, Y. Suffren, J. Hankache, N. Amstutz, L. M. Lawson Daku, E. Vauthey and A. Hauser, *Coord. Chem. Rev*., 2015, **282**-**283**, 87.
2 B. Pashaei and H. Shahroosvand, *Inorg. Chem. Com*., 2020, **112**, 107737 and references cited therein.
3 L. Conti, E. Macedi, C. Giorgi, B. Valtancoli and V. Fusi, *Coord. Chem. Rev*., 2022, **469**, 214656.
4 Y-L. Li, A-J. Li, S-L, Huang, J. J. Vittal and G-Y. Yang, *Chem. Soc. Rev*., 2023, **52**, 4725.
5 P. Reveco, R. H. Schmehl, W. R. Cherry, F. R. Fronczek and J. Selbin, *Inorg. Chem*., 1985, **24**, 4078.
6 S. U. Son, K. H. Park, Y-S. Lee, B. Y. Kim, C. H. Choi, M. S. Lah, Y. H. Jang, D-J, Jang and Y. K. Chung, *Inorg. Chem*., 2004, **43**, 6896.
7 (a) D. Schleicher, H. Leopold, H. Borrmann and T. Strassner, *Inorg. Chem*., 2017, **56**, 7217. (b) J. Soellner, I. Cisarova and T. Strassner, *Organometallics,* 2018, **37**, 4619. (c) D. G. Brown, N. Sanguantrakun, B. Schulze, U. S. Schubert and C. P. Berlinguette, *J. Am. Chem. Soc*., 2012, **134**, 12354. (d) R. T. Ryan, K. C. Stevens, R. Calabro, S. Parkin, J. Mahmoud, D. Y. Kim, D. K. Heidary, E. C. Glazer and J. P. Selegue, *Inorg. Chem*., 2020, **59**, 8882.
8 A. W. Johnson, Ylides and imines of phosphorus, Willey, 1993.
9 A. Sarbajna, V. S. V. S. N. Swamy and V. H. Gessner, *Chem. Sci*., 2021, **12**, 2016.
10 H. Schmidbaur, *Angew. Chem. Int. Ed. Engl*., 1983, **22**, 907.
11 (a) E. P. Urriolabeitia, *Top. Organomet. Chem.,* 2010, **30**, 15. (b) D. A. Valyaev and Y. Canac, *Dalton Trans.,* 2021, **50**, 16434.
12 (a) Y. Canac, C. Lepetit, M. Abdalilah, C. Duhayon and R. Chauvin, *J. Am. Chem. Soc*., 2008, **130**, 8406. (b) Y. Canac and C. Lepetit, *Inorg. Chem*., 2017, **56**, 667.
13 (a) R. Taakili, C. Barthes, A. Goëffon, C. Lepetit, C. Duhayon, D. A. Valyaev and Y. Canac, *Inorg. Chem*., 2020, **59**, 7082. (b) Y. Shi, B. W. Pan, J. S. Yu, Y. Zhou and J. Zhou, *Chem. Cat. Chem*., 2021, **13**, 129.
14 (a) A. Johnson and M. C. Gimeno, *Chem. Eur. J.,* 2020, **26**, 11256. (b) R. Visbal, N. Rosado, J. Zapata-Rivera and M. C. Gimeno, *Inorg. Chem*., 2024, **63**, 6589.
15 L. Candish, K. D. Collins, G. C. Cook, J. J. Douglas, A. Gómez-Suárez, A. Jolit and S. Keess, *Chem. Rev*., 2022, **122**, 2907.
16 M. L. Muro-Small, J. E. Yarnell, C. E. McCusker and F. N. Castellano, *Eur. J. Inorg. Chem*., 2012, 4004.
17 (a) G. J. Barbante, P. S. Francis, C. F. Hogan, P. R. Kheradmand, D. J. D. Wilson and P. J. Barnard, *Inorg. Chem*., 2013, **52**, 7448. (b) V. Leigh, W. Ghattas, R. Lalrempuia, H. Müller-Bunz, M. T. Pryce and M. Albrecht, *Inorg. Chem*., 2013, **52**, 5395.
18 J. A. M. Lummiss, W. L. McClennan, R. McDonald and D. E. Fogg, *Organometallics,* 2014, **33**, 6738.
19 M. Brissard, M. Gruselle, B. Malézieux, R. Thouvenot, C. Guyard-Duhayon and O. Convert, *Eur. J. Inorg. Chem*., 2001, 1745.
20 J. Zanzi, Z. Pastorel, C. Duhayon, E. Lognon, C. Coudret, A. Monari, I. M. Dixon, Y. Canac, M. Smietana and O. Baslé*, JACS Au*, 2024, **4**, 3049.
21 D. M. Schultz and T. P. Yoon, Science, 2014, **343**, N° 1239176.
22 J. D. Bell and J. A. Murphy, *Chem. Soc. Rev*., 2021, **50**, 9540.
23 A. G. Condie, J. C. González-Gómez and C. R. J. Stephenson, *J. Am. Chem. Soc*., 2010, **132**, 1464.
24 O. Baslé, C.-J. Li, *Green Chem*., 2007, **9**, 1047.
25 H. Bartling, A. Eisenhofer, B. König and R. M. Gschwind, *J. Am. Chem. Soc*., 2016, **138**, 11860.
26 T. Nevesely, M. Wienhold, J. J. Molloy and R. Gilmour, *Chem. Rev*., 2022, **122**, 2650.
27 S. E. Chérif, A. Ghosh, S. Chelli, I. M. Dixon, J. Kraiem and S. Lakhdar, *Chem. Science*, 2022, **13**, 12065.